Supporting Information

Exciplex-based multi-stimuli-responsive luminescent materials: photo-recoverable mechanochromic luminescence for reusable paper applications

Fengqi Zhang,[a] Yongsheng Yang,*[a] Tingting Lu,[a] Ke Hu[a] and Zhen Zhao*[ab]

[a] Institute of Catalysis for Energy and Environment, College of Chemistry and Chemical Engineering, Shenyang Normal University, Shenyang 110034, China. E-mail: yangys@synu.edu.cn; zhenzhao@cup.edu.cn

[b] State Key Laboratory of Heavy Oil Processing, China University of Petroleum, Beijing 102249, China.

Table of Contents

Fig. S10 (a) Reversible variation of the maximum emission intensity and (b) Commission Internationale de l'Eclairage (CIE) color coordinates for complex **1** under alternate treatment of grinding and fuming by CH_3CN. (c) Solid-state UV-vis absorption spectra of **1-P**, **1-G** and **1-F**.

Fig. S11 SEM images of (a) **1-C**, (b) **1-P**, (c) **1-G** and (d) **1-F** samples.

Fig. S12 Theoretical calculation simulation of IR spectra for complex **1**.

Fig. S13 (a) PXRD patterns and (b) IR spectra of **1-P** under time-dependent irradiation. (c) PXRD patterns and (d) IR spectra of **1-G** under time-dependent irradiation.

Fig. S14 XPS spectra of **1-P** before and after irradiation under 365 nm.

Fig. S15 XPS spectra of **1-G** before and after irradiation under 365 nm.

Fig. S16 (a) Reversible variation of the emission spectra, (b) Reversible variation of the maximum emission intensity and (c) Commission Internationale de l'Eclairage (CIE) color coordinates for complex **1** under alternate treatment of grinding and UV irradiation.

Fig. S17 (a) Luminescence photos of **1-H** and **1-OH** under 365 nm UV lamp. (b) Reversible variation of the emission spectra for complex **1** under alternate treatment of HCl and NH_3 fuming. (c) PXRD patterns of **1-H** and **1-OH**. (d) IR spectra of **1-H** and **1-OH**.

Fig. S18 (a) Time-resolved emission decay curves for **1-H** (λ_{ex} = 360 nm and λ_{em} = 490 nm) under ambient conditions. (b) Time-resolved emission decay fitting curves for **1-H**. (c) Time-resolved emission decay curves for **1-OH** (λ_{ex} = 360 nm and λ_{em} = 450 nm) under ambient conditions. (d) Time-resolved emission decay fitting curves for **1-OH**.

Fig. S19 (a) Reversible variation of the maximum emission intensity and (b) Commission Internationale de l'Eclairage (CIE) color coordinates for complex **1** under alternate treatment of HCl and NH_3 fuming. (c) Solid-state UV-vis absorption spectra of **1-P**, **1-H**, **1-OH** and **9-HAC**.

Fig. S20 (a) The emission spectra, (b) UV-vis spectra, (c) PXRD patterns and (d) IR spectra of **1-H** under time-dependent irradiation.

Fig. S21 The calculated spatial distributions of LUMO and HOMO of 9-HAC and IM ligands at the B3LYP/6-31G(d) level.

Fig. S22 The luminescence photographs of the complete luminescent response and recovery process involving "writing-erasing-retention".

Fig. S23 The photoluminescent emission spectra (a) and the normalized photoluminescence emission spectra (b) of **1-P**, **1-G**, **1-UV** and **1-Dark**.

Table S1 Crystallographic data and structure refinement details of **1**.

Table S2 Bond lengths and angles related to the coordination environment.

Table S3 Photophysical data of **1-C** and **1-P** in the solid state.

Movie S1 Schematic video of photo-printing.

Movie S2 Schematic video of force-writing and photo-erasing.

Movie S3 Schematic video of recyclable writing and erasing.

3. References

1. Experimental section

1.1 Materials and Reagents

Analytically pure $Cd(NO_3)_2 \cdot 4H_2O$, anthracene-9-carboxylic acid (9-HAC), imidazole (IM) and other reagents used as purchased without further purification.

1.2 Characterization

Single-crystal X-ray diffraction data were collected on a Bruker SMART APEX II diffractometer with graphite-monochromated Mo Kα radiation (λ = 0.71073 Å) at 296 K. CrysAlisPro[1] was used for data collection, data reduction and empirical absorption correction. The crystal structure was solved by direct methods, using OLEX2 program and least-squares refined with SHELXL-2015[2] using anisotropic thermal displacement parameters for all non-hydrogen atoms. The crystallographic data for $Cd_2(9\text{-}AC)_4(IM)_2$ is listed in **Table S1**. Selected bond lengths and angles are listed in **Table S2**. Crystallographic data for the complex structure in this work has also been deposited with the Cambridge Crystallographic Data Centre (CCDC) as deposition nos. CCDC 2204005 (available free of charge, on application to the CCDC, 12 Union Rd., Cambridge CB2 1EZ, U.K.; e-mail deposit@ccdc.cam.ac.uk). Powder X-ray diffraction analyses (PXRD) patterns were collected on a Rigaku Ultima-IV automated diffraction system with Cu Kα radiation (λ = 1.5406 Å). Measurements were made in a 2ϑ range of 5−50° at room temperature with a step of 0.02° (2ϑ) and a counting time of 0.2 s/step. The operating power was 40 kV and 50 mA. Simulated curves of PXRD were exported by the single-crystal data and diffraction-crystal module of the Mercury (Hg) program available free of charge via the Internet at http://www.iucr.org. The fluorescence spectra and time-resolved emission decay curves were measured on a Hitachi F-7100 fluorescence spectrophotometer at room temperature, and the temperature-dependent measurements were conducted using the same spectrometer equipped with an Orient KOJI TAP-02 high-temperature fluorescence analyzer (300 °C). The photoluminescent lifetimes (τ) of all samples were calculated by fitting the decay curve with a two-exponential decay function of $I(t)=A_1\exp(-t/\tau_1)+A_2\exp(-t/\tau_2)$, where A_1, A_2 and τ_1, τ_2 represent the amplitudes and lifetimes of the individual components for two-exponential decay profiles, respectively. The absolute emission quantum yield (QY) values were measured at room temperature using an Edinburgh quantum yield measurement system equipped with a 150-W xenon lamp coupled to a monochromator for wavelength discrimination, an integrating sphere as the sample chamber, and a multichannel analyzer for signal detection.

Ultraviolet-visible (UV-vis) absorption spectra were recorded by using a Hitachi UH4150 spectrometer with $BaSO_4$ as a reflectance scaffold. The Fourier transform infrared (FT-IR) spectra for samples were obtained utilizing the Nicolet 380 spectrophotometer in the range of 400-4000 cm^{-1} to investigate the functional groups. The thermogravimetry analysis (TGA) experiments were performed on a VersaTherm TGA instrument from room temperature to 600 °C under flowing N_2 with a heating rate of 10 °C/min. Sample preparations for the TGA were carried out under air. The morphologies and particle sizes were obtained by scanning electron microscopy (SEM) images on Hitachi S-4800. Electron paramagnetic resonance (EPR) spectroscopy was measured on a Bruker-300 EPR spectrometer. X-ray photoelectron spectroscopy (XPS) measurements were performed on a PerkinElmer PHI-1600 ESCA spectrometer using a Mg Kα (hv = 1253.6 eV) X-ray source. The binding energies were calibrated using the C 1s peak of contaminant carbon (BE = 284.0 eV) as an internal standard. For the light irradiation experiments, A Xe lamp (150 W) was equipped to prepare the samples for luminescence performance measurement, a UV lamp (365 nm, 24 W) for IR, PXRD, UV-vis, luminous photos and a UV lamp (365 nm, 100 W) for EPR.

1.3 Theoretical Calculations

The Hirshfeld surfaces and 2D fingerprint plots were calculated by using Crystal Explorer 17.5.[3] The molecular structures were optimized and characterized as energy minima by the Becke three-parameter exchange functional with the Lee–Yang–Parr correction functional (B3LYP[4-5]) in the Gauss 16 package.[6] The density functional theory (DFT) was performed to optimize the geometries of the ground state with the 6-31G(d) basis set for C, H, O and N atoms, and LANL2DZ basis set for the Cd atom. The calculation of the infrared absorption frequencies was carried out at the same level.

1.4 Preparation of samples

1.4.1 Preparation of metal-organic complex 1:

A mixture of 0.2 mmol 9-HAC (0.044 g), 0.2 mmol IM (0.014 g) and 6 mL CH_3CN solvent were added to the beaker to prepare “A” solution, which was stirred at a suitable speed for 4 hours on a magnetic stirrer. The 0.5 mmol $Cd(NO_3)_2{\cdot}4H_2O$ (0.154 g) was dissolved in 8 mL deionized water to form “B” solution. After the “A” solution was stirred for 3 hours, the “B” solution was added and stirred for another 3 hours to finally obtain a light-yellow clarified solution. The solution after the reaction was filtered into a Schering bottle and sealed with a sealing film. A number of small holes

were punched on the sealing film to control the evaporation rate of the solvent. After a week, yellow block crystals were precipitated at the bottom of the Schering bottle. After filtration, washing and drying, the sample was finally obtained. Yield: 75% (based on 9-HAC). IR spectrum of $Cd_2(9\text{-}AC)_4(IM)_2$ (KBr pellets, cm^{-1}): 3129(w), 3053(w), 2954(w), 2865(w), 2107(w), 1595(vs), 1540(w), 1502(w), 1489(w), 1441(m), 1418(m), 1391(s), 1318(s), 1277(w), 1258(w), 1227(w), 1183(w), 1160(w), 1140(w), 1104(w), 1073(s), 1014(w), 981(w), 961(w), 947(w), 886(m), 866(m), 839(w), 819(w), 794(m), 762(m), 732(vs), 650(s), 619(m), 595(m), 560(m), 520(m), 462(m), 425(vs).

1.4.2 Preparation of 1-G:

$Cd_2(9\text{-}AC)_4(IM)_2$ was ground in a mortar to obtain a light-yellow powder sample. IR spectrum of $Cd_2(9\text{-}AC)_4(IM)_2$-G (KBr pellets, cm^{-1}): 3129(w), 3051(w), 2106(w), 1598(s), 1540(m), 1502(w), 1485(w), 1442(m), 1421(w), 1388(s), 1321(s), 1278(w), 1260(w), 1225(w), 1181(w), 1158(w), 1141(w), 1104(w), 1076(m), 1013(w), 981(w), 961(w), 949(w), 886(m), 866(m), 840(w), 821(w), 794(w), 782(w), 762(m), 730(vs), 647(s), 619(m), 597(m), 560(m), 520(m), 463(w), 425(s).

1.4.3 Preparation of 1-F:

$Cd_2(9\text{-}AC)_4(IM)_2$-G was fumigated with CH_3CN solvent to obtain a light-yellow powder sample. IR spectrum of $Cd_2(9\text{-}AC)_4(IM)_2$-F (KBr pellets, cm-1): 3131(w), 3055(w), 2954(w), 2865(w), 1598(vs), 1540(w), 1502(w), 1485(w), 1439(m), 1422(m), 1392(s), 1320(s), 1277(w), 1258(w), 1227(w), 1183(w), 1160(w), 1140(w), 1104(w), 1076(s), 1016(w), 981(w), 963(w), 951(w), 886(m), 866(m), 841(w), 821(w), 802(w), 794(w), 762(m), 730(vs), 650(s), 619(m), 595(m), 560(m), 520(m), 462(m), 425(vs).

1.4.4 Preparation of 1-H:

$Zn_2(9\text{-}AC)_4(IM)_2$ was fumigated with concentrated HCl to obtain a yellow powder sample. IR spectrum of $Zn_2(9\text{-}AC)_4(IM)_2$-H (KBr pellets, cm^{-1}): 3137(w), 3055(w), 1675(s), 1608(m), 1482(w), 1444(w), 1424(m), 1386(w), 1318(w), 1292(m), 1254(s), 1225(w), 1176(w), 1143(w), 1099(w), 1070(m), 1012(w), 954(w), 916(w), 887(m), 858(w), 840(w), 790(m), 732(vs), 636(m), 597(m), 558(w), 520(w), 472(w), 433(m).

1.4.5 Preparation of 1-OH:

$Zn_2(9\text{-}AC)_4(IM)_2$-H was fumigated with concentrated $NH_3{\cdot}H_2O$ to obtain a light-yellow powder sample. IR spectrum of $Zn_2(9\text{-}AC)_4(IM)_2$-OH (KBr pellets, cm^{-1}): 3137(w), 3055(w), 1610(s), 1552(m), 1489(w), 1441(m), 1402(s), 1393(s), 1318(s), 1270(m), 1254(m), 1238(w), 1180(w), 1141(w),

1103(w), 1074(s), 1016(w), 958(w), 919(w), 890(m), 861(m), 842(m), 794(m), 765(m), 736(vs), 649(s), 601(m), 562(w), 524(m), 475(m), 437(m).

2. Supplementary Figures and Tables

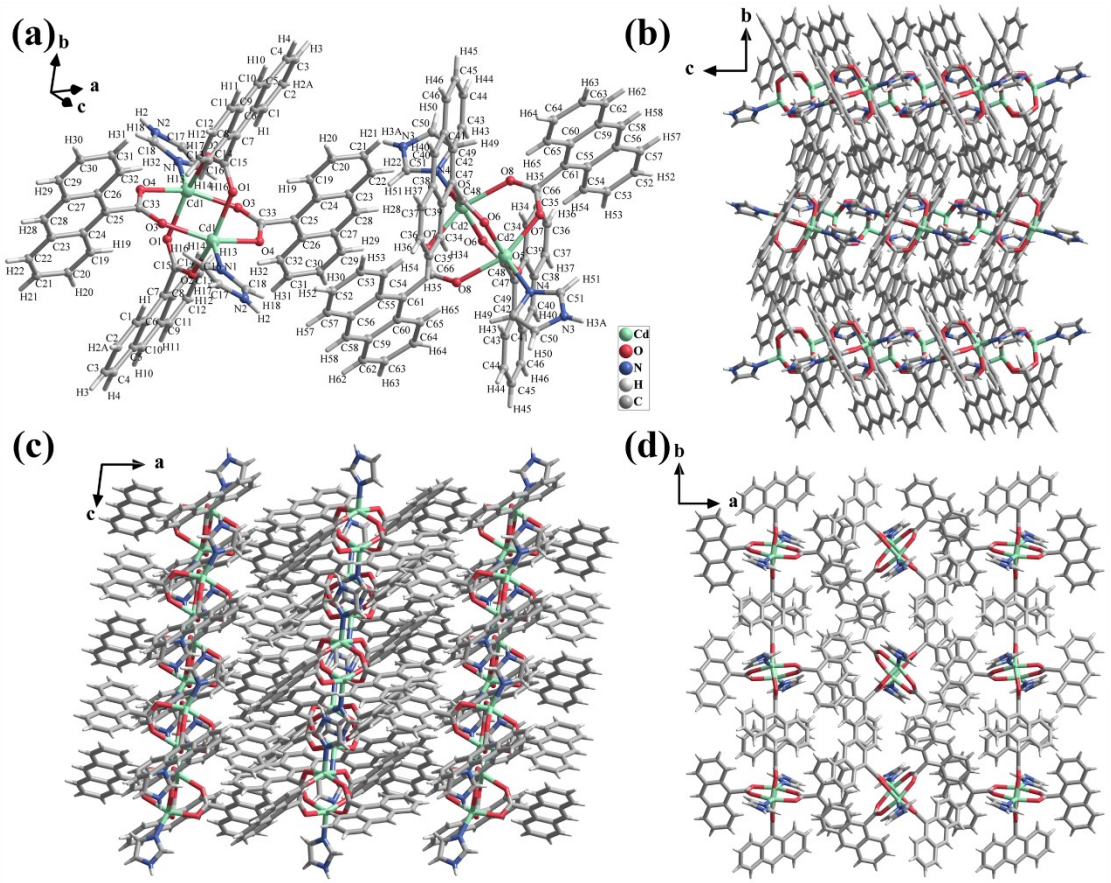

Fig. S1 (a) Molecular structure of **1** showing the atom numbering scheme. Three-dimensional stacking diagram of *a*-axis (b), *b*-axis (c) and *c*-axis (d) perspectives, respectively.

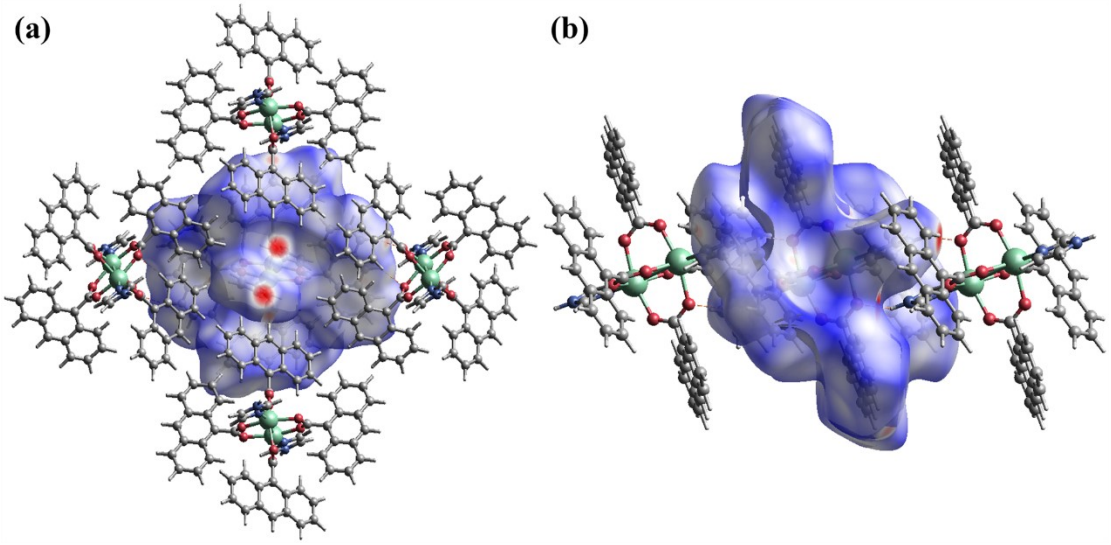

Fig. S2 Hirshfeld surface of **1**.

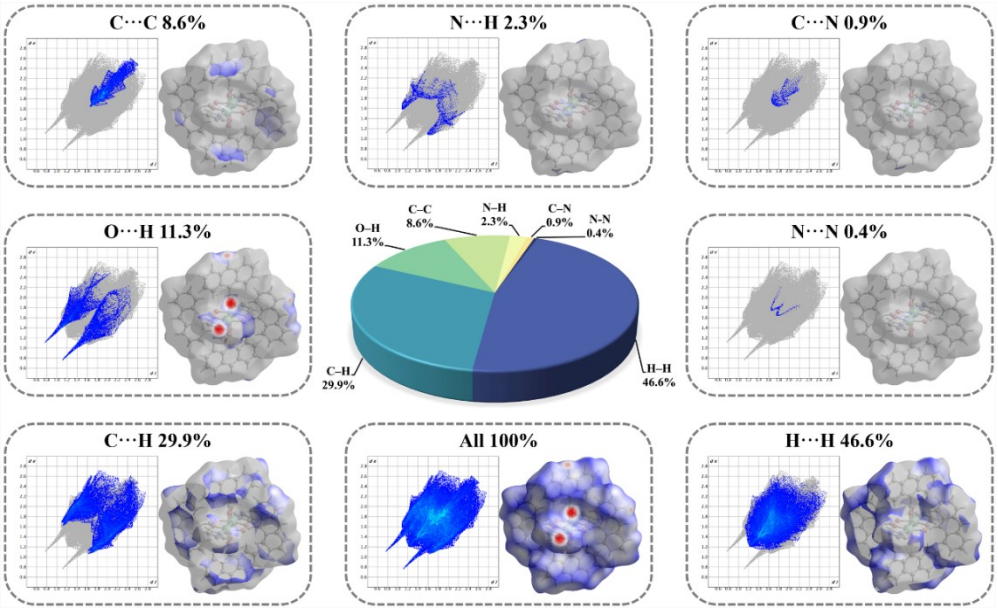

Fig. S3 The 2D fingerprint plots and relative contributions to the Hirshfeld surface areas for the various intermolecular contacts in **1**.

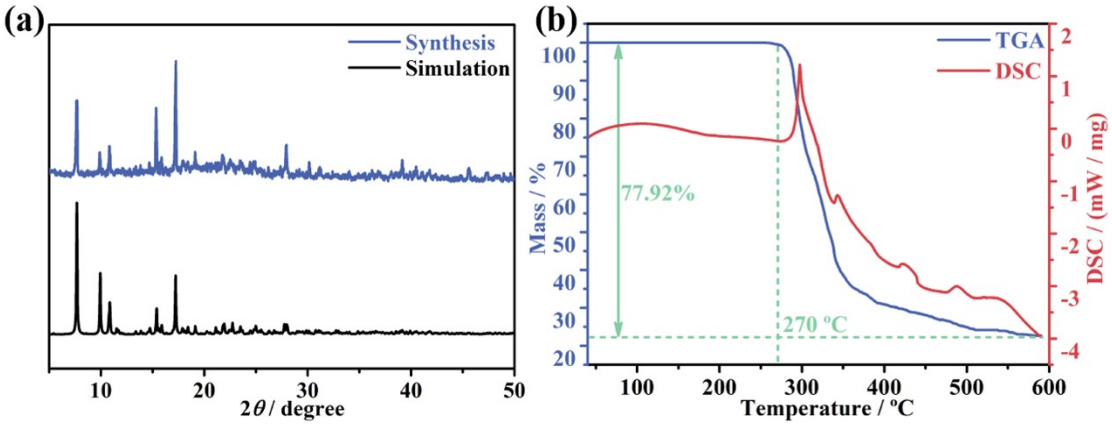

Fig. S4 (a) The PXRD patterns for **1**. (b) TGA (blue line) and DSC (red line) curves for **1**.

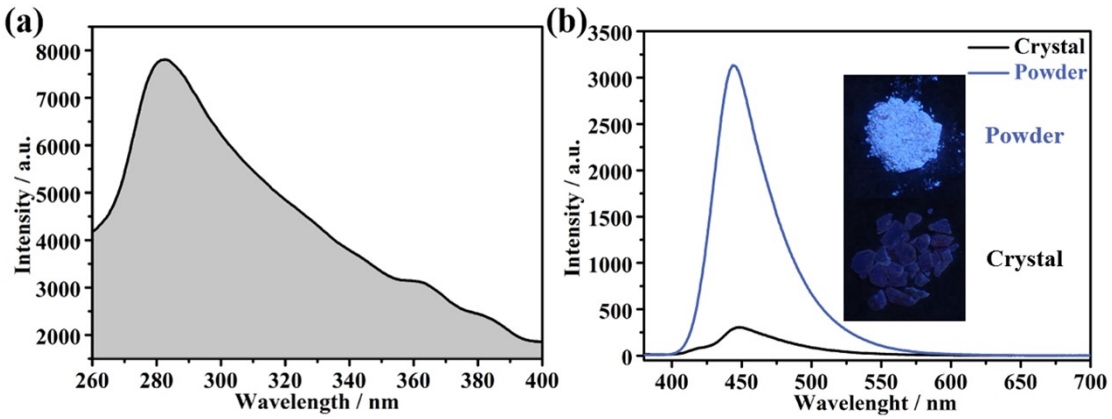

Fig. S5 (a) Room-temperature solid-state excitation spectrum of **1** (λ_{em} = 450 nm) and (b) Room-temperature solid-state photoluminescent emission spectra of **1** (λ_{ex} = 360 nm) in its powder and crystal states.

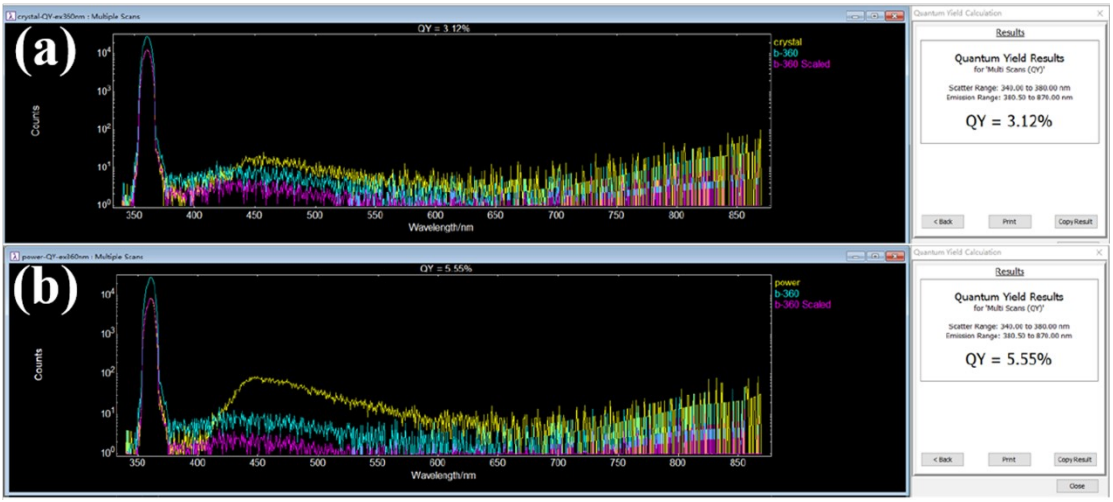

Fig. S6 The measurements of quantum yield for **1-C** (a) and **1-P** (b) at 298 K.

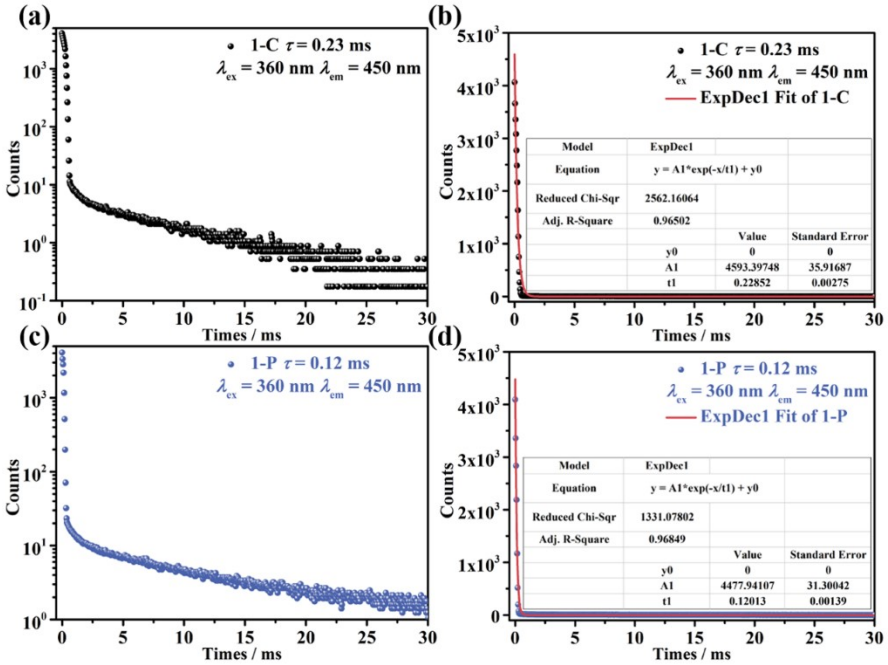

Fig. S7 (a) Time-resolved emission decay curves for **1-C** (λ_{ex} = 360 nm and λ_{em} = 450 nm) under ambient conditions. (b) Time-resolved emission decay fitting curves for **1-C**. (c) Time-resolved emission decay curves for **1-P** (λ_{ex} = 360 nm and λ_{em} = 450 nm) under ambient conditions. (d) Time-resolved emission decay fitting curves for **1-P**.

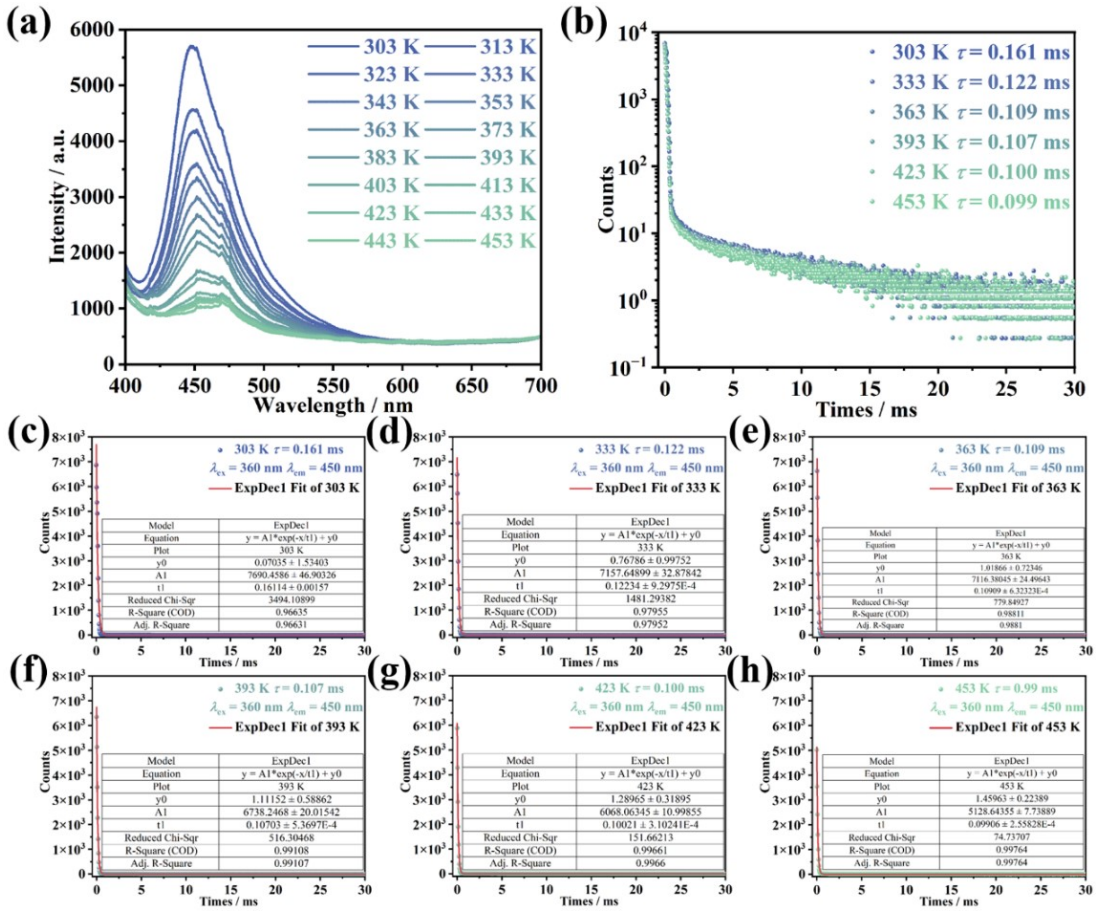

Fig. S8 (a) Emission spectra for complex **1** measured at temperatures from 303 to 453 K. (b) Time-resolved emission decay curves for complex **1** (λ_{ex} = 360 nm and λ_{em} = 450 nm) measured at temperatures from 303 to 453 K. (c-h) Time-resolved emission decay fitting curves for complex 1 measured at temperatures from 303 to 453 K.

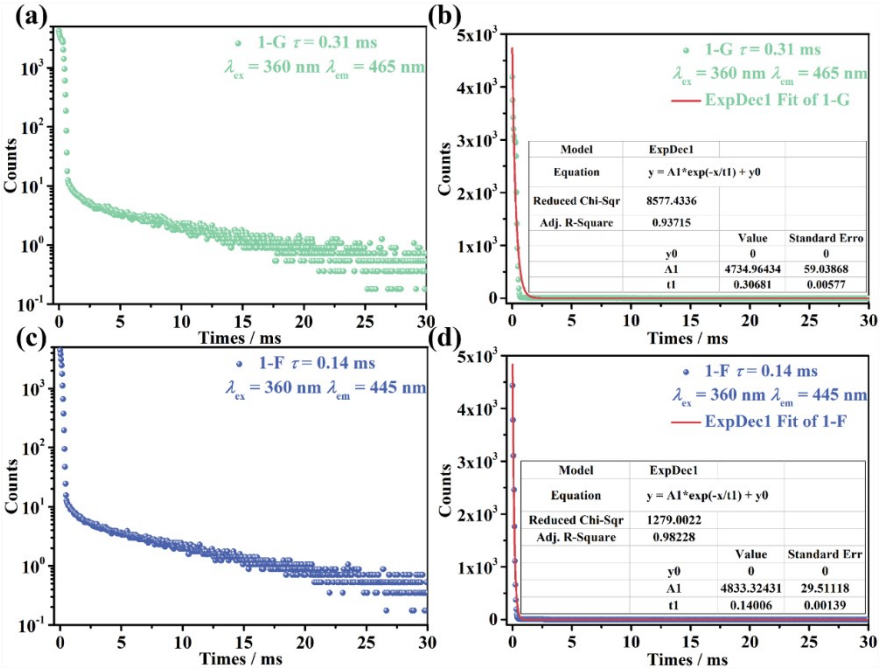

Fig. S9 (a) Time-resolved emission decay curves for **1-G** (λ_{ex} = 360 nm and λ_{em} = 465 nm) under ambient conditions. (b) Time-resolved emission decay fitting curves for **1-G**. (c) Time-resolved emission decay curves for **1-F** (λ_{ex} = 360 nm and λ_{em} = 445 nm) under ambient conditions. (d) Time-resolved emission decay fitting curves for **1-F**.

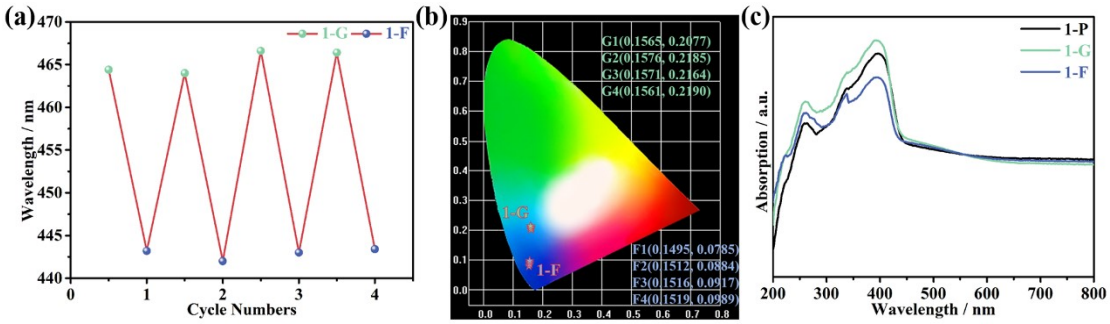

Fig. S10 (a) Reversible variation of the maximum emission intensity and (b) Commission Internationale de l'Eclairage (CIE) color coordinates for complex **1** under alternate treatment of grinding and fuming by CH_3CN. (c) Solid-state UV-vis absorption spectra of **1-P**, **1-G** and **1-F**.

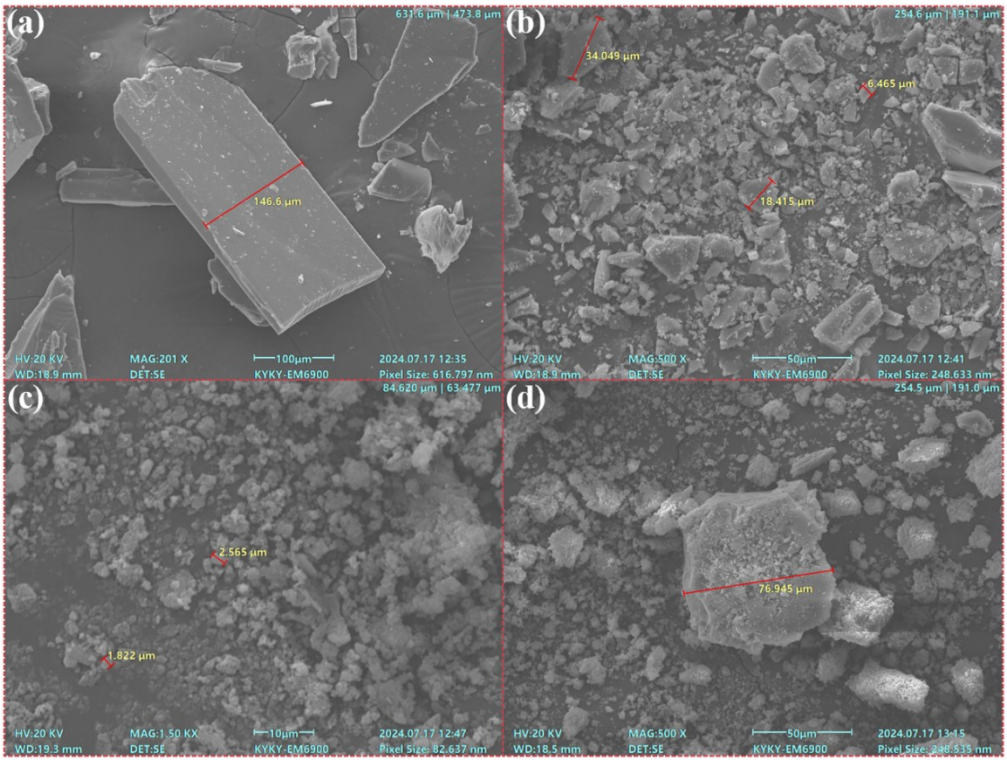

Fig. S11 SEM images of (a) **1-C**, (b) **1-P**, (c) **1-G** and (d) **1-F** samples.

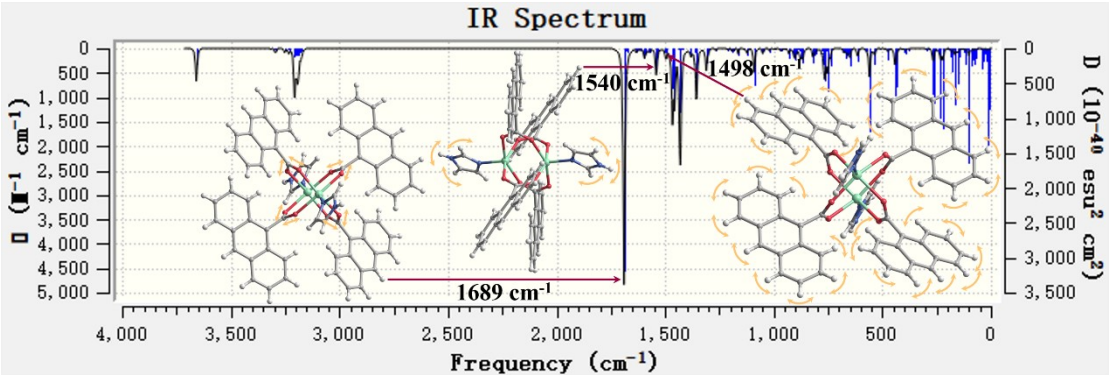

Fig. S12 Theoretical calculation simulation of IR spectra for complex **1**.

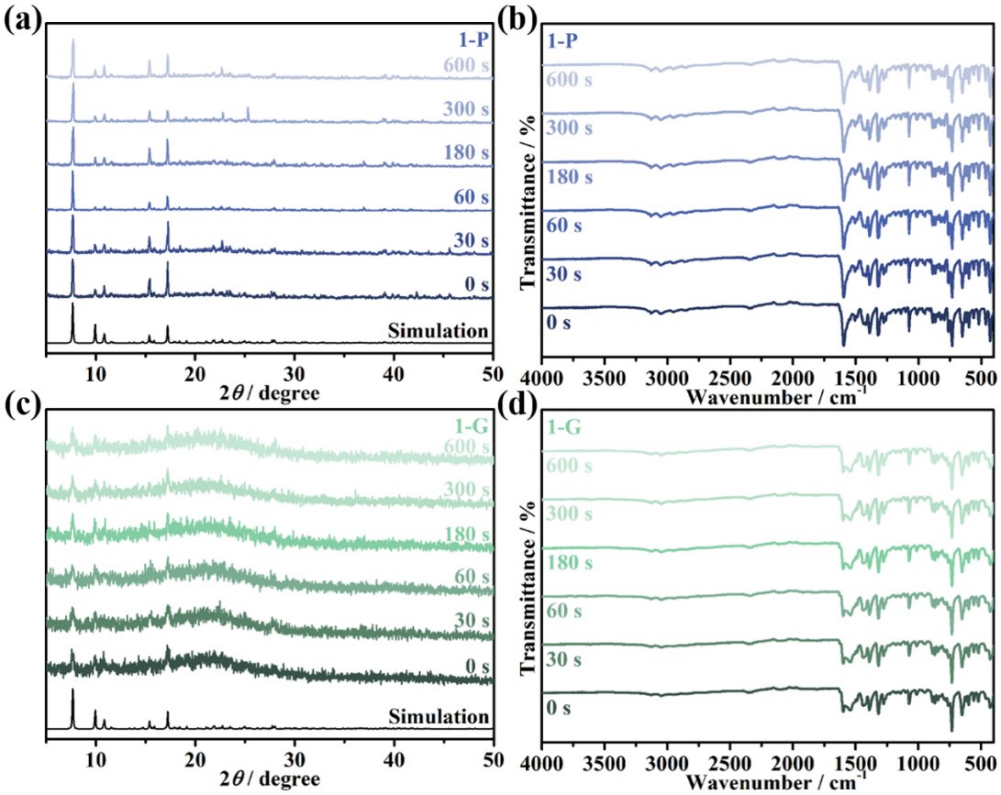

Fig. S13 (a) PXRD patterns and (b) IR spectra of **1-P** under time-dependent irradiation. (c) PXRD patterns and (d) IR spectra of **1-G** under time-dependent irradiation.

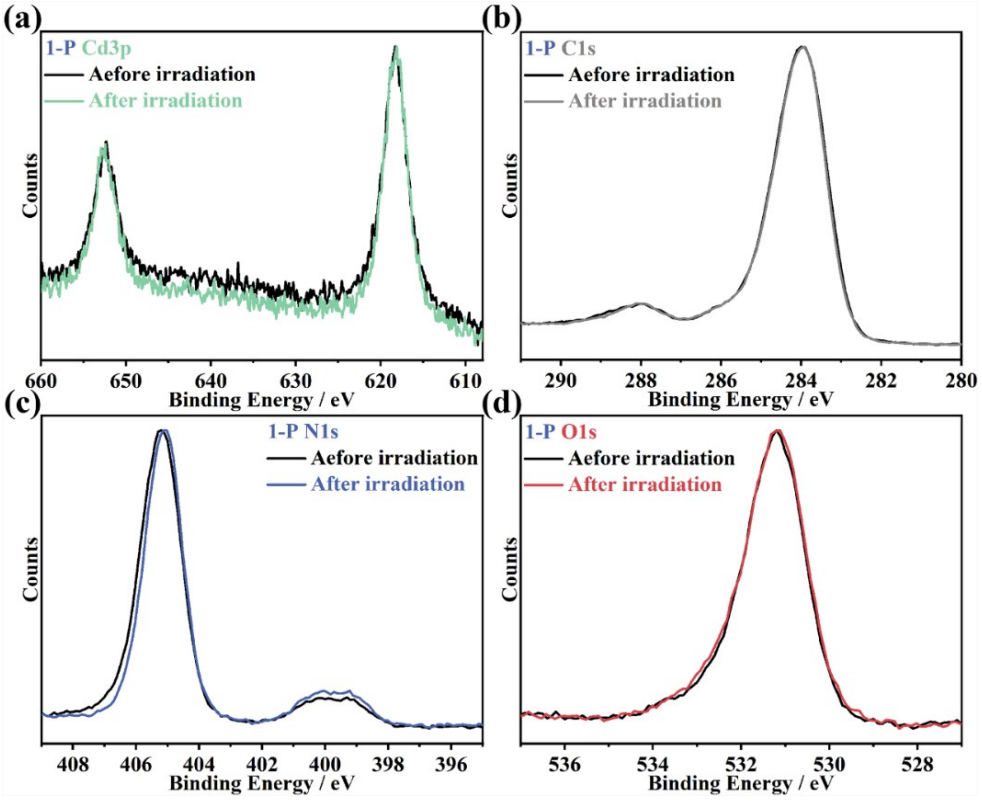

Fig. S14 XPS spectra of **1-P** before and after irradiation under 365 nm.

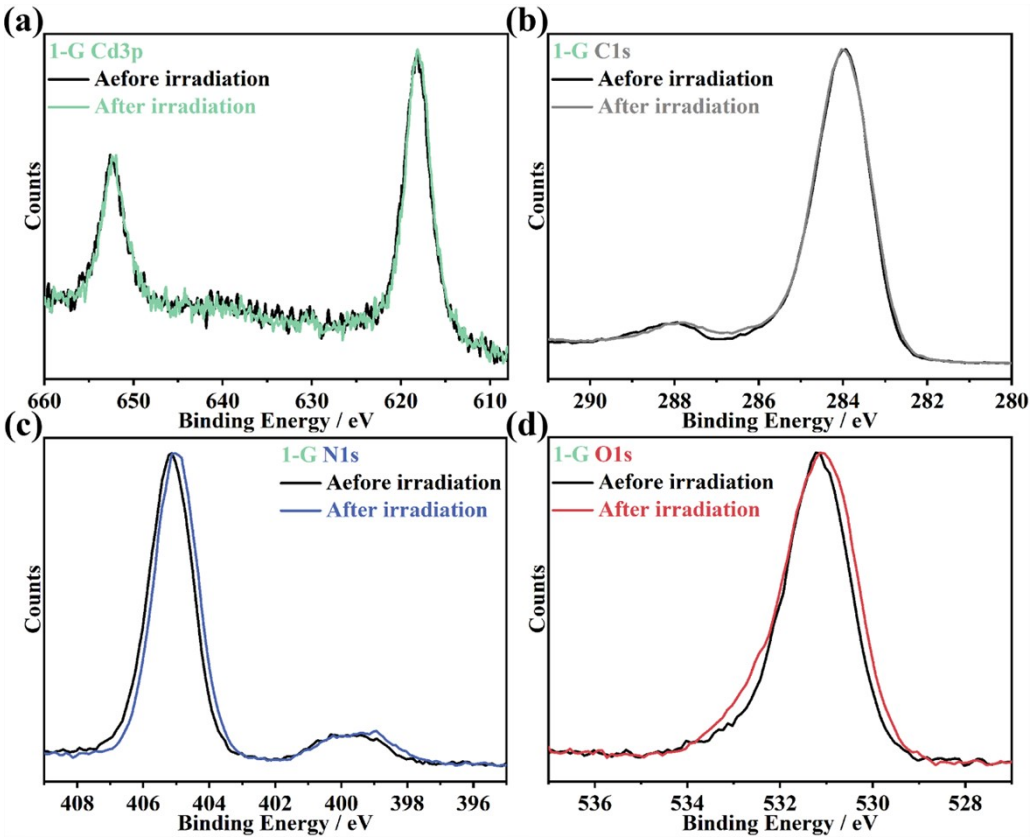

Fig. S15 XPS spectra of **1-G** before and after irradiation under 365 nm.

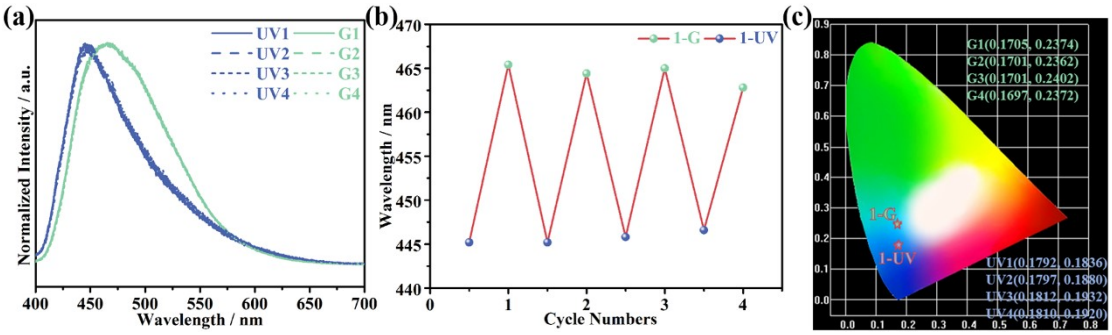

Fig. S16 (a) Reversible variation of the emission spectra, (b) Reversible variation of the maximum emission intensity and (c) Commission Internationale de l'Eclairage (CIE) color coordinates for complex **1** under alternate treatment of grinding and UV irradiation.

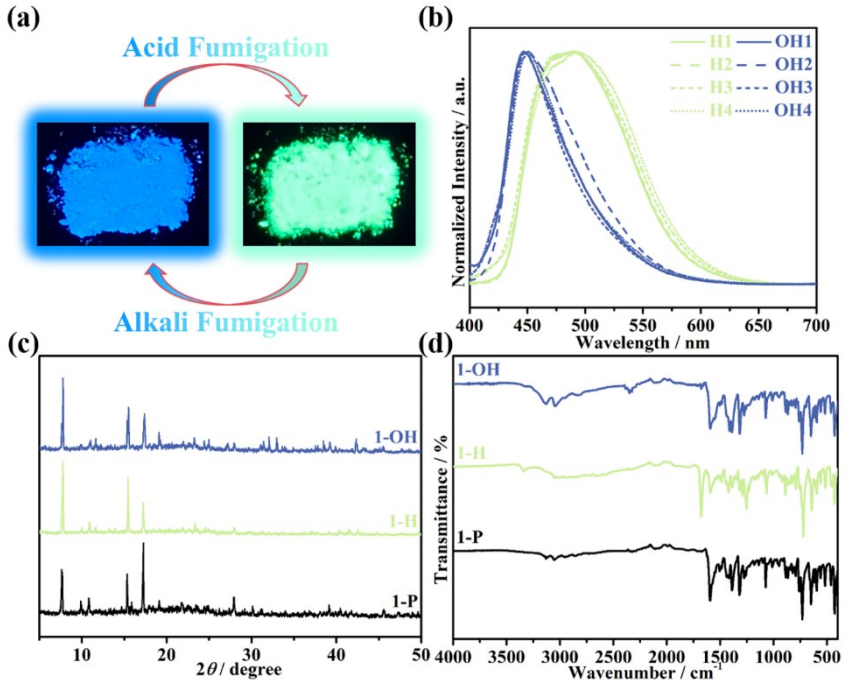

Fig. S17 (a) Luminescence photos of **1-H** and **1-OH** under 365 nm UV lamp. (b) Reversible variation of the emission spectra for complex **1** under alternate treatment of HCl and NH_3 fuming. (c) PXRD patterns of **1-H** and **1-OH**. (d) IR spectra of **1-H** and **1-OH**.

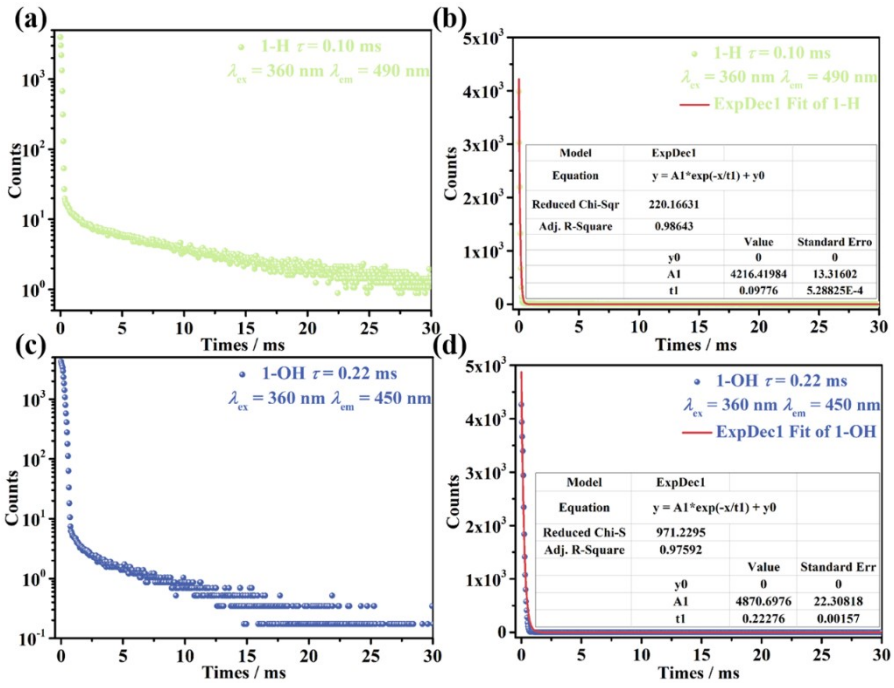

Fig. S18 (a) Time-resolved emission decay curves for **1-H** (λ_{ex} = 360 nm and λ_{em} = 490 nm) under ambient conditions. (b) Time-resolved emission decay fitting curves for **1-H**. (c) Time-resolved emission decay curves for **1-OH** (λ_{ex} = 360 nm and λ_{em} = 450 nm) under ambient conditions. (d) Time-resolved emission decay fitting curves for **1-OH**.

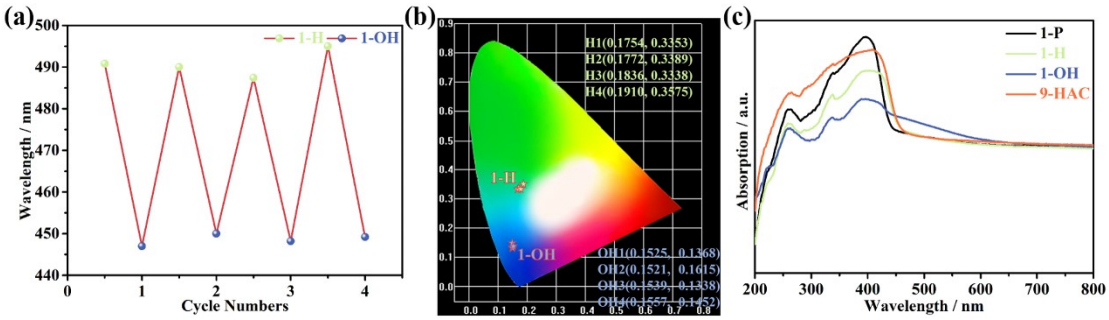

Fig. S19 (a) Reversible variation of the maximum emission intensity and (b) Commission Internationale de l'Eclairage (CIE) color coordinates for complex **1** under alternate treatment of HCl and NH_3 fuming. (c) Solid-state UV-vis absorption spectra of **1-P**, **1-H**, **1-OH** and **9-HAC**.

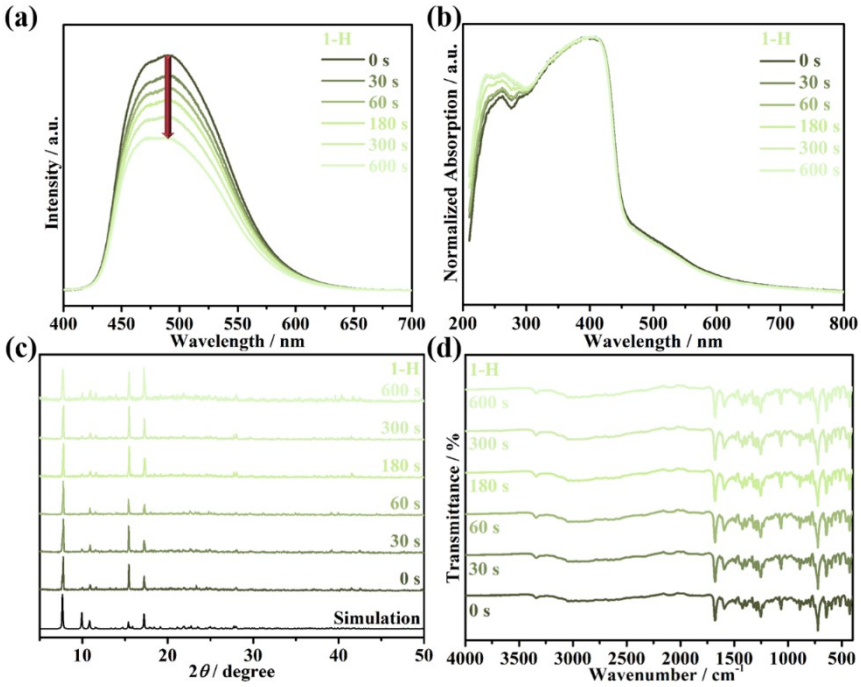

Fig. S20 (a) The emission spectra, (b) UV-vis spectra, (c) PXRD patterns and (d) IR spectra of **1-H** under time-dependent irradiation.

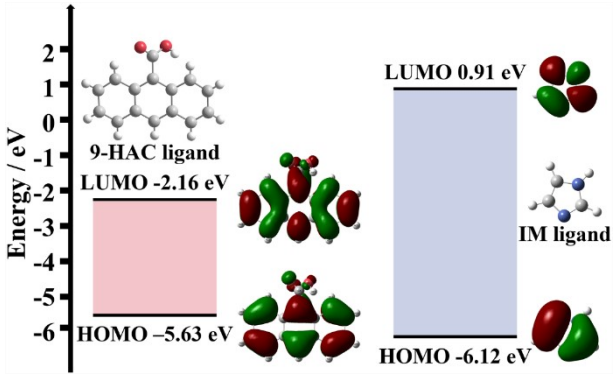

Fig. S21 The calculated spatial distributions of LUMO and HOMO of 9-HAC and IM ligands at the B3LYP/6-31G(d) level.

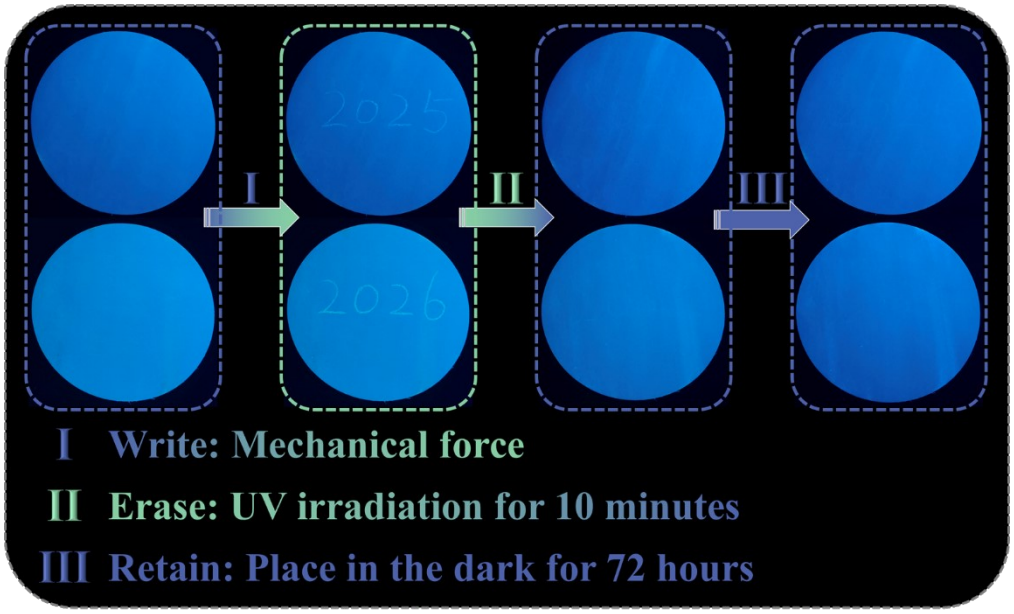

Fig. S22 The luminescence photographs of the complete luminescent response and recovery process involving "writing-erasing-retention".

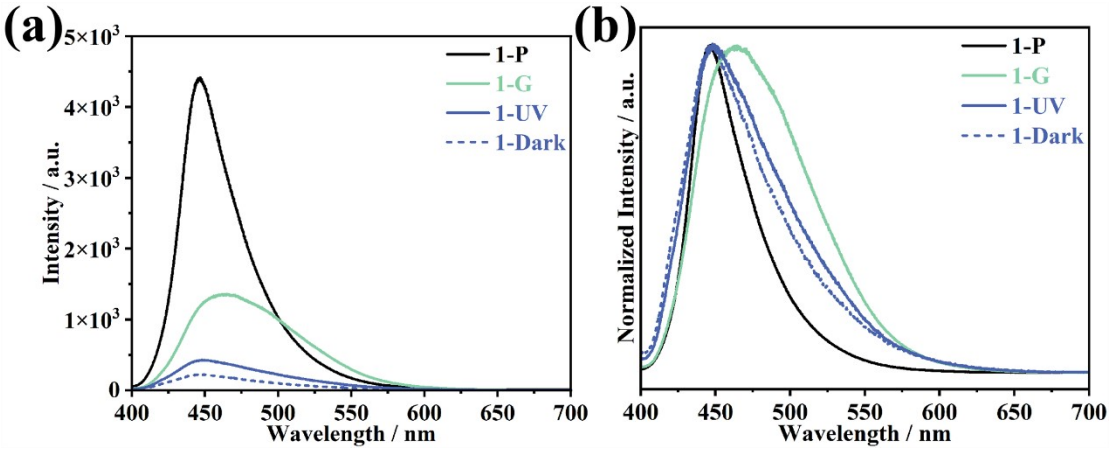

Fig. S23 The photoluminescent emission spectra (a) and the normalized photoluminescence emission spectra (b) of **1-P**, **1-G**, **1-UV** and **1-Dark**.

Table S1 Crystallographic data and structure refinement details of **1**.

Complex	$Cd_2(9\text{-}AC)_4(IM)_2$	***Z***	4
Formula	$C_{66}H_{44}N_4O_8Cd_2$	D_{calc} **(mg/m³)**	1.550
Mr	1245.85	**ϑ Range (°)**	2.219-25.041
Temperature (K)	296.15	***F* (000)**	2512
Crystal system	monoclinic	**Data/restraint/parameters**	9411 / 1032 / 721
Space group	*P*21/*c*	**Reflections collected**	121925
Crystal size (mm)	0.06 × 0.05 × 0.04	**Independent reflections**	9411
***a* (Å)**	23.1894(11)	**Goodness-of-fit on F2**	1.027
***b* (Å)**	23.0008(9)	R_{int}	0.0614
***c* (Å)**	10.0936(4)	R_1**[I>2σ(I)]**	0.0427
***α* (°)**	90	wR_2**[I>2σ(I)]**	0.0799
***β* (°)**	97.3350(10)	R_1**(all data)**	0.0652
***γ* (°)**	90	wR_2**(all data)**	0.0901
***V*(Å³)**	5339.6(4)	**Residuals(e Å⁻³)**	0.705, -0.846

$R_1 = \Sigma||F_o|-|F_c||/\Sigma|F_o|$, $wR_2 = [\Sigma w(F_o^2-F_c^2)^2/\Sigma w(F_o^2)^2]^{1/2}$

Table S2 Bond lengths and angles related to the coordination environment.

Bond lengths (Å)		**Bond angles (º)**			
Cd1–O1	2.276(3)	O1–Cd1–O2	154.60(11)	O3–Cd1–O4	155.95(13)
Cd1–O2	2.224(3)	O1–Cd1–O3	88.48(12)	N1–Cd1–O1	97.09(12)
Cd1–O3	2.243(3)	O1–Cd1–O4	83.15(12)	N1–Cd1–O2	108.20(12)
Cd1–O4	2.212(3)	O2–Cd1–O3	97.77(13)	N1–Cd1–O3	96.83(13)
Cd1–N1	2.197(3)	O2–Cd1–O4	87.35(13)	N1–Cd1–O4	106.53(13)
Cd2–O5	2.233(3)	O5–Cd2–O6	155.39(11)	O7–Cd2–O8	155.97(12)
Cd2–O6	2.285(3)	O5–Cd2–O7	87.57(13)	N4–Cd2–O5	105.81(13)
Cd2–O7	2.229(3)	O5–Cd2–O8	91.12(13)	N4–Cd2–O6	98.43(12)
Cd2–O8	2.237(3)	O6–Cd2–O7	81.68(12)	N4–Cd2–O7	105.91(13)
Cd2–N4	2.210(3)	O6–Cd2–O8	89.86(13)	N4–Cd2–O8	97.53(13)

Table S3 Photophysical data of **1-C** and **1-P** in the solid state.

Complex	***T*/K**	$\lambda_{em}{}^a$**/nm**	Φ^b	τ^c**/ms**	$k_r{}^d$**/s⁻¹**	$k_{nr}{}^e$**/s⁻¹**
1-C	298 K	450	3.12%	0.23	1.36×10^2	4.21×10^3
1-P	298 K	450	5.55%	0.12	4.63×10^2	7.87×10^3

[a] Emission Maxima. [b] Emission quantum yields. [c] Emission lifetimes.

[d] Radiative rate constants, $k_r = \Phi/\tau$. [e] Non-radiative rate constants, $k_{nr} = (1-\Phi)/\tau$.

3. References

1. CrysAlisPro, Rigaku Oxford Diffraction, *Version 1.171.39.6a*, Rigaku Corp., Oxford, UK 2015.

2. G. M. Sheldrick, *Acta Crystallogr., Sect. A*, 2008, **64**, 112−122.

3. M. J. Turner, et al. *CrystalExplorer Version 17.5*, University of Western Australia, 2017.

4. A. D. Becke, *Phys. Rev. A*, 1988, **38**, 3098−3100.

5. A. D. Becke, *J. Chem. Phys.*, 1993, **98**, 5648−5652.

6. M. Frisch, et al. *Gaussian 16, Revision A.03*, Gaussian, Inc. Wallingford CT, 2016.